Femtosecond x-ray diffraction from an aerosolized beam of protein nanocrystals

arXiv:1702.04014v2 [physics.bio-ph] 15 Feb 2017

Salah Awel,[a,b] Richard A. Kirian,[e] Max O. Wiedorn,[a,c] Kenneth R. Beyerlein,[a] Nils Roth,[a] Daniel A. Horke,[a,b] Dominik Oberthür,[a] Juraj Knoska,[a] Valerio Mariani,[a] Andrew Morgan,[a] Luigi Adriano,[d] Alexandra Tolstikova,[a,c] P. Lourdu Xavier,[a,h] Oleksandr Yefanov,[a] Andrew Aquila,[g] Anton Barty,[a] Shatabdi Roy-Chowdhury,[e] Mark S. Hunter,[g] Daniel James,[e] Joseph S. Robinson,[g] Uwe Weierstall,[e] Andrei V. Rode,[f] Saša Bajt,[d] Jochen Küpper[a,b,c] and Henry N. Chapman[a,b,c]*

[a]*Center for Free-Electron Laser Science, Deutsches Elektronen-Synchrotron DESY, Notkestraße 85, 22607 Hamburg, Germany,* [b]*The Hamburg Center for Ultrafast Imaging, University of Hamburg, Luruper Chaussee 149, 22761 Hamburg, Germany,* [c]*Department of Physics, University of Hamburg, Luruper Chaussee 149, 22761 Hamburg, Germany,* [d]*Photon Science, Deutsches Elektronen-Synchrotron DESY, Notkestraße 85, 22607 Hamburg, Germany,* [e]*Arizona State University, Tempe , Arizona, USA,* [f]*Laser Physics Centre, Research School of Physics and Engineering, Australian National University, ACT 2601, Canberra, Australia,* [g]*Linac Coherent Light Source (LCLS), SLAC National Accelerator Laboratory, 2575, Sand Hill Road, Menlo Park, CA 94025, USA, and* [h]*Max-Planck Institute for the Structure and Dynamics of Matter, Luruper Chaussee 149, 22761 Hamburg, Germany.*

E-mail: henry.chapman@desy.de

Abstract

We demonstrate near-atomic-resolution Bragg diffraction from aerosolized single granulovirus crystals using an x-ray free-electron laser. The form of the aerosol injector is nearly identical to conventional liquid-microjet nozzles, but the x-ray-scattering background is reduced by several orders of magnitude by the use of helium carrier gas rather than liquid. This approach provides a route to study the weak diffuse or lattice-transform signal arising from small crystals. The high speed of the particles is particularly well suited to upcoming MHz-repetition-rate x-ray free-electron lasers.

1. Introduction

Serial femtosecond crystallography (SFX) allows the imaging of biomolecular samples from crystallized targets that are notoriously difficult, or sometimes impossible, to study with synchrotron sources. The SFX technique was enabled by x-ray free-electron lasers (x-ray FELs); their ultrashort and highly intense pulses, with typical pulse energies of $\sim$1 mJ, pulse durations of $\sim$10 fs, and wavelength of $\sim$100 pm, allow one to overcome the fundamental problem of x-ray induced radiation damage (Neutze *et al.*, 2000; Boutet *et al.*, 2012). Furthermore, x-ray FELs enable novel time-resolved studies with femtosecond temporal resolution, 100 picometer spatial resolution, and at physiological temperatures. A variety of remarkable results from SFX measurements using x-ray FELs are summarized in recent reviews and special issues (Spence *et al.*, 2012; Schlichting & Miao, 2012; Barty *et al.*, 2013; Patterson, 2014; Schlichting, 2015; Muniyappan *et al.*, 2015).

Typical SFX measurements are performed on microcrystals that produce intense Bragg reflections at high signal-to-noise ratio, which led to its rapid success and widespread adoption (Chapman *et al.*, 2011; Boutet *et al.*, 2012). Intense Bragg reflections allow the use of sample delivery techniques that surround the crystals in dense media, such as liquid microjets (DePonte *et al.*, 2008; Weierstall, 2014), viscous extrusion injectors (Weierstall *et al.*, 2014) or solid substrates (Frank *et al.*, 2014). This is in stark contrast to non-crystalline imaging approaches, which tend to suffer from extremely weak scattering signals (Küpper *et al.*, 2014; Aquila *et al.*, 2015; Yang *et al.*, 2016). Non-crystalline particles must be efficiently delivered to the x-ray focus in a vacuum environment and in isolation from other potential scattering sources. This can be achieved, for example, through aerodynamic focusing (Bogan *et al.*, 2008; Bogan *et al.*, 2010*a*; Bogan *et al.*, 2010*b*). In certain cases background scattering from a dense surrounding medium is highly undesirable even for experiments on crystalline samples. For example, imaging techniques have been developed to utilize the faint continuous diffraction signal in regions between the intense Bragg reflections (Ayyer *et al.*, 2016). For sufficiently small crystals, the spatial coherence associated with XFEL pulses provides a direct route to solving the crystallographic phase problem without the need for prior knowledge or additional measurements (Spence *et al.*, 2011; Kirian *et al.*, 2015*b*).

Here, we demonstrate high-resolution x-ray diffraction from isolated protein nanocrystals delivered via a convergent-nozzle aerosol injector (Kirian *et al.*, 2015*a*) into the FEL focus. We show that the aerosol delivery produces extremely low background scattering signals compared to a conventional liquid jet. This aerosol injector has essentially the same size and form as the gas-dynamic virtual nozzles that are commonly used to produce liquid jets for SFX experiments (Beyerlein *et al.*, 2015) and, hence, can be installed using standard liquid-jet mountings available at x-ray facilities.

As shown in our previous work, convergent nozzles can produce aerosolized beams of sub-micrometer particles with a full-width at half maximum diameter < 5 µm and particle velocities on the order of a few hundred meters per second, depending on particle size and operating conditions. This high velocity is well-suited to the MHz repetition rates of upcoming XFEL sources.

2. Experimental methods

This proof-of-principle experiment was performed on natural Cydia pomonella granulovirus particles of approximately $200 \times 200 \times 400$ nm^3 in size that consist of a central virus body surrounded by a crystalline granulin protein shell. They infect invertebrates such as the codling moth (Cydia pomonella) (Jehle *et al.*, 2006). The granulovirus particles used in this study were purified from a biopesticide solution (Certis Madex HP) using a method described elswhere (Oberthür *et al.*, 2016) and suspended in water at a concentration of 10^{11} particles/ml prior to injection. Previous SFX experiments have recorded diffraction to 2.1 Å resolution from granulovirus particles delivered to the x-ray beam in a gas-focused liquid jet (Gati *et al.*, 2017).

Diffraction measurements were performed in the nanofocus chamber at the coherent x-ray imaging (CXI) (Liang *et al.*, 2015) instrument at the Linac Coherent Light Source (LCLS). A mist of liquid microdrops containing protein crystals was generated from a ceramic injection-molded gas-dynamic virtual nozzle (GDVN) (Beyerlein *et al.*, 2015). The drops were contained in a cylindrical nebulization chamber of approximately 40 mm inner diameter (ID) and 150 mm length. The liquid jet was continuously monitored with a visible-light CCD through glass viewports on the nebulization chamber. From the nebulization chamber, the aerosolized crystals were transported through conductive silicone rubber tubing (Simolex, 6.3 mm inner diameter, 30 cm length), which was coupled to the standard "nozzle rod" leading from the chamber

exterior to the x-ray focal point, Figure 1 (a). This nozzle rod is a 1.2 m long stainless steel rod with a 6.3 mm inner diameter that is used to transfer liquid-jet injectors mounted on the tip in and out of the main experimental chamber without breaking vacuum (Weierstall *et al.*, 2012).

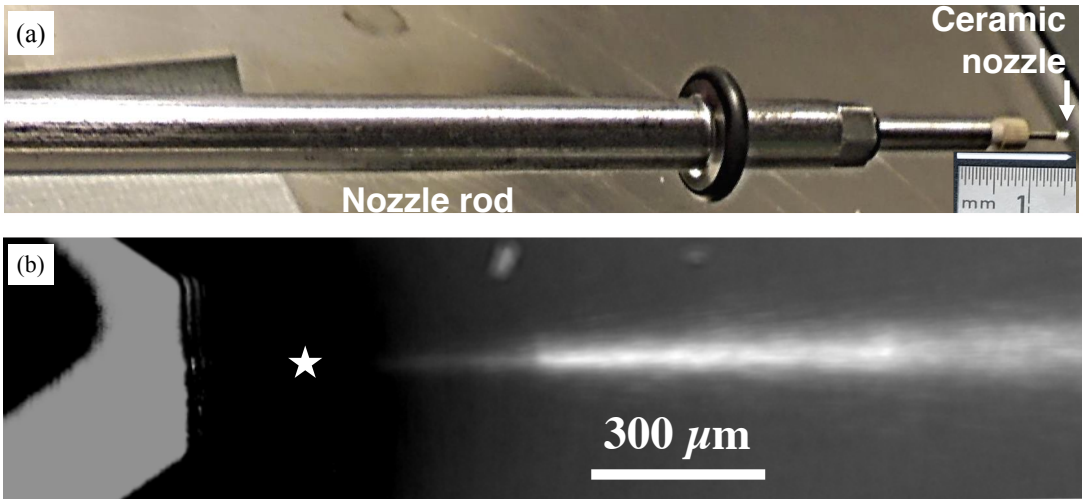

Fig. 1. (a) The converging ceramic nozzle mounted on the nozzle rod. (b) Time integrated image of a laser-illuminated stream of GV particles exiting the convergent nozzle aerosol injector, recorded using the in-line microscope at the CXI end station. The image of the convergent nozzle tip is seen in the left portion of the image, and the approximate x-ray focal point is indicated by the star. This image was formed by averaging over 3.7 minutes, with a running median background subtracted from each frame.

The pressure upstream of the aerosol nozzle was maintained at approximately 0.1–1 bar. This pressure depended on the gas flow rate of the GDVN and the flow restricting exit diameter of the aerosol nozzle. Helium was used as the GDVN focusing gas, and it also carried the crystals through the nozzle rod to the convergent aerosol injector. The typical helium mass flow rate of the ceramic GDVN nozzles was in the range of 10–60 mg/min, limited by the pumping speed and vacuum requirements of the main experimental chamber.

At a mass flow rate of 30 mg/min we calculated that it would take approximately

15 s for the crystals to traverse the nozzle rod and flexible tubing. The time that crystals spend in the nebulization chamber is difficult to assess, but it takes approximately 240 s to evacuate one chamber-volume of gas. Crystals were indeed observed to exit the injector for several minutes after the GDVN was switched from a solution of crystals to pure water.

We monitored the crystal injection through direct optical imaging of scattered laser light from injected particles (Awel *et al.*, 2016). A pulsed Nd:YLF laser (527 nm, ∼3 mJ per 150-ns pulse, 120 Hz) was focused to a ∼0.8 mm spot within the aerosol stream, and scattered light observed through the in-line microscope available at CXI (Questar long distance microscope, model: QM-1 MK III, NA = 0.05 at 750 mm objective distance). Images were recorded using an OPAL-4000 CCD camera and stored at 30 Hz. In order to avoid possible ablation of the crystals by the illumination laser, and to protect the detector from scattered optical light, the laser timing was adjusted to illuminate particles only in the time interval between the end of x-ray detector read-out and the start of next diffraction acquisition. Figure 1 (b) shows a 3.7 min time-averaged optical image of the particles exiting the injector. We estimate that the particles moved at speeds of approximately 300 m/s when they exit the injector and arrived at the x-ray interaction point within a flight-time of less than 1 µs. The nozzle tip is seen to the left of this image, and the approximate x-ray focal point is indicated by the star. The particle stream could not be observed at points close to the nozzle tip because direct scattering from the nozzle tip saturated the imaging CCD.

3. Laboratory injector characterization

In our laboratory test setup we tested both, 15 ° and 30 °, converging-nozzle tips (Kirian *et al.*, 2015*a*) using a mounting scheme similar to that used at CXI. Aerosols were

transported from the nebulization chamber to the injector tip using Swagelok stainless steel tubing (4 mm inner diameter and 700 mm long). The GDVN was operated at flow rates of 2.7 µl/min and 28 mg/min, for liquid sample and helium respectively. A GV concentration of approximately 1.6×10^9 particles/ml was used (50 times diluted from the stock solution that was used at the CXI experiment). The particle concentration was measured using a NanoSight (model LM14C) particle sizer. Assuming a typical initial droplet diameter of ~ 2 µm (as measured in the laboratory) created by the GDVN and no clustering or multiple particles per drop, this flow rate corresponds to the generation of drops at a rate of 1.3 MHz, and an "entrance rate" of aerosol particles of 72 kHz (i.e. the rate at which particles enter the aerosol injector).

The imaging setup used for visualizing particles was described in detail previously (Awel *et al.*, 2016). Briefly, it comprised a Nd:YLF laser (Spectra Physics Empower ICSHG-30, 527 nm, pulse duration 100 ns, repetition rate 1 kHz, pulse energy 20 mJ) to illuminate particles and a high-frame-rate CMOS camera (Photron SA4) to record images. The camera exposure time was set to 20 ms, such that each frame contains 20 pulses of the 1 KHz Nd:YLF laser illumination.

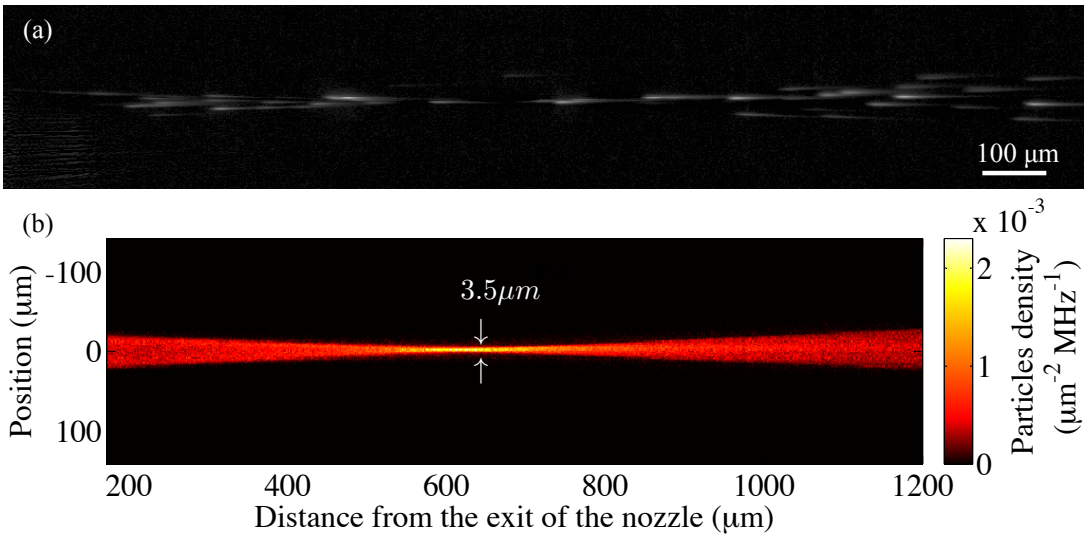

Fig. 2. A high-magnification view of a beam of a GV particles. (a) A single exposure showing streaked images of GV particles caused by the 100 ns laser illumination (b) The average 2D particle density determined from the centroids of individual particle images as the one shown in (a).

A single exposure raw image of particles emerging from the convergent injector is shown in Figure 2 (a). Centroid positions of individual particle streaks contained in 23,500 frames, measured over ∼13 min of data acquisition, were used to produce the projected two-dimensional particle density map shown in Figure 2 (b). Specifically, this entrance-rate-corrected particle column-density D, i. e., the particle column-density projected along the optical imaging axis, Figure 2 (b), per particles entering into the front end of the injector, is equal to

$$D = \frac{N_p}{A \times R} \,, \tag{1}$$

where N_p is the average number of particles that fall within a spatial bin of area A, and R is the entrance rate at which particles enter the injector. Note that N_p is corrected for the number of recorded images and the number of laser illumination pulses per image; since we intend to use femtosecond illumination, N_p represents the expected particle counts at an instant in time, not a time-integration over many

exposures. D is normalized by the entrance rate R because the centroiding analysis we performed required the measurement of isolated particle images and hence much lower concentration than would be used in a typical XFEL measurement. Importantly, the number of particles that exit the injector may be less than the number that enter. The ratio of these two numbers is often referred to as the transmission efficiency of the injector. The observed quantity D defined above implicitly includes transmission efficiency; it represents a *lower bound* on the particle density for a given entrance rate R.

We define the hit fraction H_{fraction} as the fraction of x-ray pulses that produce an acceptable diffraction pattern. For the situation we consider here, we may write H_{fraction} as

$$H_{\text{fraction}} \approx \frac{\pi}{4} D (d_x + d_p)^2 R = \frac{\pi}{4} \frac{(d_x + d_{\text{p}})^2}{A} N_{\text{p}} \tag{2}$$

where d_x is the diameter of the x-ray beam, d_p is the diameter of the particle. This formula applies to cases in which both d_x and d_p are much smaller than the overall particle beam diameter.

The maximum of D recorded in the lab, i. e., at the focus of the particle beam, Figure 2 (b), was $D \approx 2.2 \times 10^{-3} \mu\text{m}^{-2}\text{MHz}^{-1}$. This number suggests that the maximum hit fraction to be expected in our XFEL diffraction measurements is $H_{\text{fraction}} \approx 0.2$ % ($d_x \approx 150$ nm, $d_p \approx 300$ nm, and $R \approx 1.2$ MHz). This predicted hit fraction is much higher than the one we actually obtained, as discussed in the next section.

4. Results and discussion

x-ray diffraction data was recorded for a total of 1.3 hours, including time for aligning the aerosol injector with respect to the x-ray beam. All measurements were conducted at a photon energy of 8.01 keV and an estimated average pulse energy of 4.2 mJ (prior to the ∼30-50 % beamline transmission losses) (Boutet, 2016).

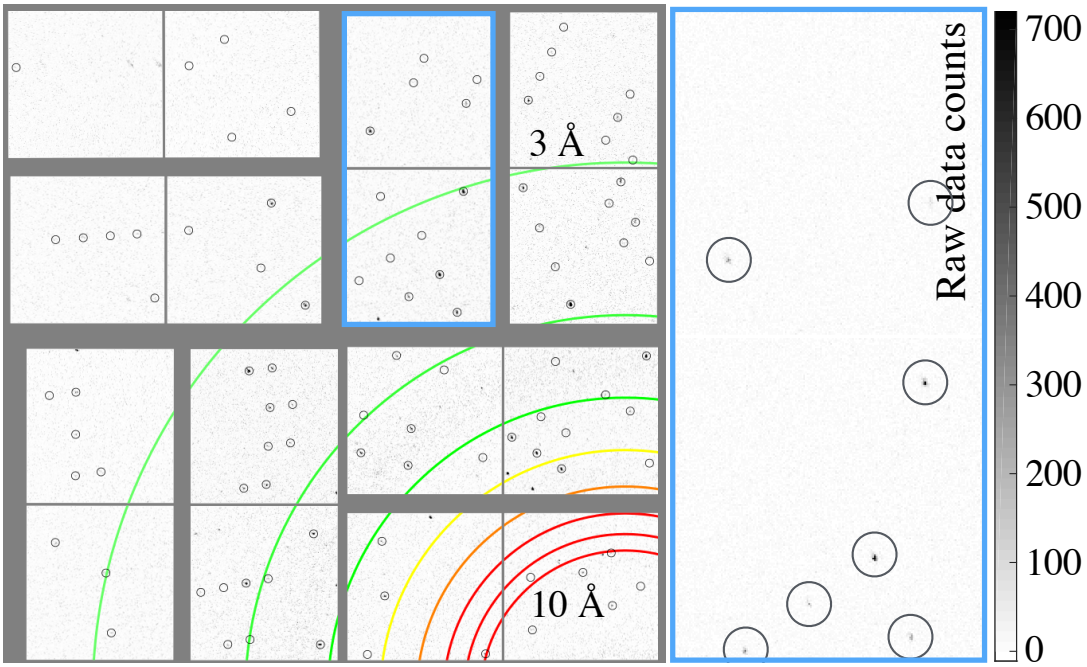

Fig. 3. One detector quadrant of an indexed diffraction pattern obtained from aerosolized GV crystals. The colored rings indicate the resolution from 1 nm to 300 pm, in steps of 100 pm. The gray circles in the left-hand panel indicate the expected locations of Bragg peaks as determined by auto-indexing in the CrystFEL software suite (White *et al.*, 2012). The right-hand panel shows expanded view of an individual detector tile, marked by the blue rectangle on the left. Circles in this expanded-view panel indicate peaks that are easily recognizable by eye.

The CSPAD detector was located at a distance of 127.9 mm from the target. Figure 3 shows one quadrant of a recorded diffraction pattern from an aerosolized GV crystal, where only detector dark current has been subtracted.

To assess the background scatter in these aerosol diffraction experiments, and to compare it to typical liquid jet studies, we show the radial profiles of the total scattered intensity for aerosol and liquid jet diffraction in Figure 4(a) and (b), respectively.

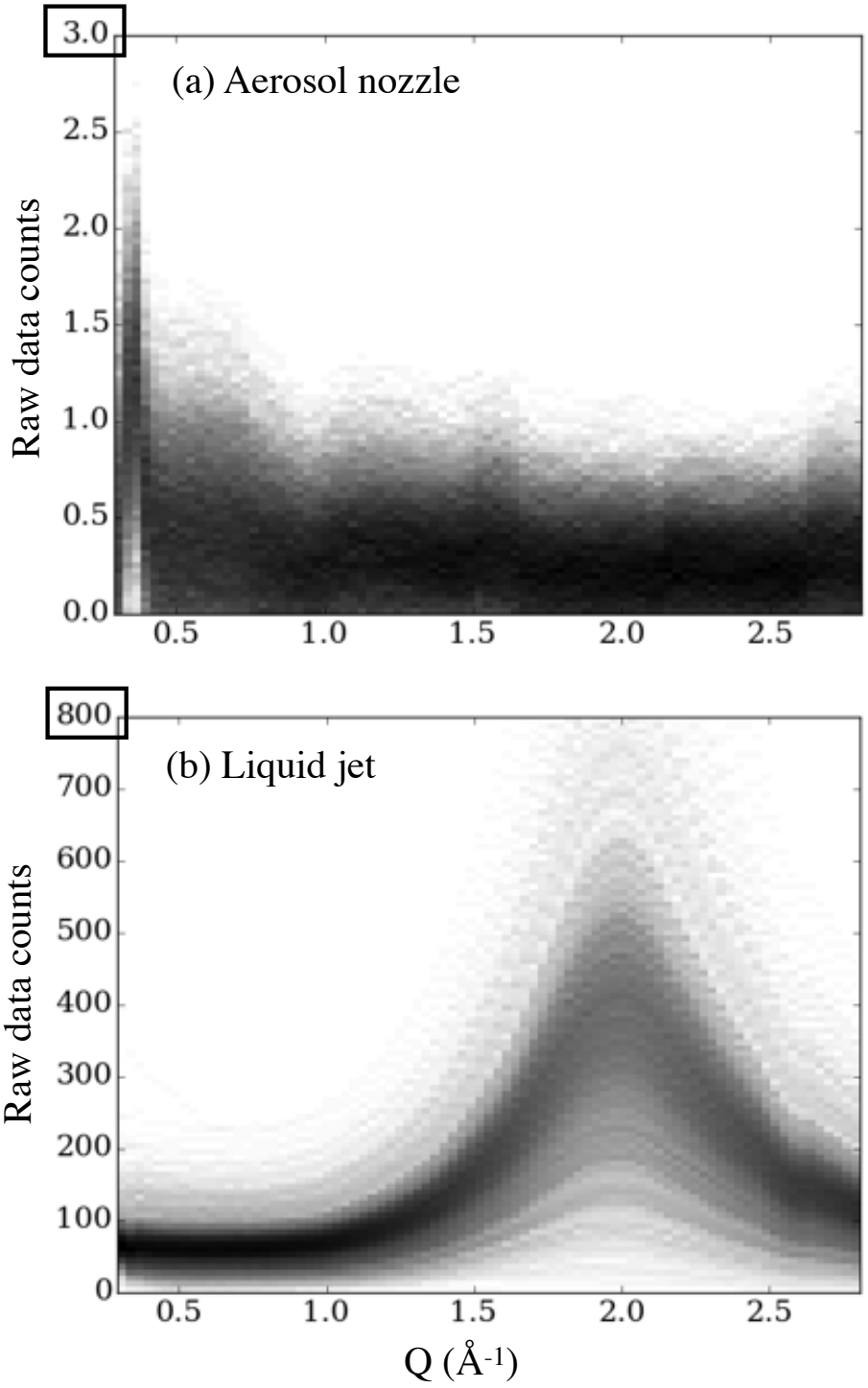

Fig. 4. Histogram of 4,500 background radial intensity profiles for (a) an aerosol injector and (b) a liquid jet flowing at 20 µl/minute. The horizontal axis is $Q = 4\pi \sin(\theta/2)/\lambda$, where θ is the scattering angle (equal to twice the Bragg angle) and λ is the wavelength.

The result from the liquid jet data will be published in (Oberthür *et al.*, 2016). The XFEL pulse properties and detector settings were identical for both datasets since the liquid-jet data were collected in the experiment directly preceding the aerosol experiment presented here.

These distributions were assembled by extracting the shot-by-shot radially averaged intensity profiles from 4,500 patterns for both the aerosol injector and a liquid-jet injector. An average dark image, recorded with the x-rays blocked, was subtracted from each frame. Figure 4(a) shows a histogram of the 4,500 radial intensity profiles obtained with aerosol diffraction from the convergent nozzle injector, whereas Figure 4(b) shows the same for a liquid jet, operated at a flow rate of 20 µl/minute, corresponding to a jet diameter of approximately 5 µm diameter. These histograms show that the background arising from liquid-water microjet scatter under typical conditions is approximately 100–1000-fold higher than the background arising from the helium carrier gas in the aerosol jet. Typical liquid flow rates to produce a stable jet range from 5–30 µl/min, depending on the viscosity and surface tension of the liquid and the nozzle geometry. The volume of liquid that interacts with the x-ray beam scales roughly as the square root of the volumetric flow rate, assuming the x-ray beam to be smaller in diameter than the liquid jet, and assuming that the velocity of the liquid does not vary with the volumetric flow rate (Beyerlein *et al.*, 2015).

During the total of 1.3 hours of data collection, a total of 33 hits from GV were recorded, corresponding to a hit fraction of ~ 0.006 %. 24 patterns (73 % of hits) were indexed using the CrystFEL (White *et al.*, 2012) software suite. Autoindexing failed on patterns that appeared to consist of multiple crystals clumped together. We expect the hit fraction for our aerosol injector to be significantly lower than a typical liquid jet (about 1-10%) because of the ∼25-fold higher particle speed of the aerosol beam. However, our recorded hit fraction was still significantly lower than the

0.2 % that we estimated from our laboratory measurements. We speculate that this discrepancy is partly caused by the 1.2 m long aerosol transport tube, which allows for greater particle diffusion losses when compared to our laboratory apparatus. In future work, the aerosol transmission efficiency can be improved by reducing the overall transportation tube length, increasing the volumetric flow rate of carrier gas, or by the addition of aerodynamic lenses within the transport tube, which would maintain particles near the center of the transport tube.

With a micro-focused particle beam, hit fractions are highly sensitive to the relative positioning of the injector nozzle with respect to the x-ray beam. This is further compounded by the fact that our injector produces a convergent, focused particle beam, rather than a collimated beam. Our principle diagnostic for particle beam positioning was direct imaging of scattered light, which proved to be both useful and necessary, but we suspect that most of the visible particles were clumps of crystals that were not necessarily indicative of the aerodynamics of smaller isolated crystals. This suspicion arises due to the large variations in particle image intensities, which should be nearly uniform as observed previously in the laboratory. The imaging sensitivity was lower at CXI than in our laboratory measurements primarily because of the smaller acceptance angle of the objective lens (NA = 0.05 compared to NA = 0.28), and for that reason it was ultimately necessary to perform a two-dimensional scan of the injector position in an effort to optimize the spatial overlap between particle beam focus and x-rays. The overall imaging sensitivity can readily be increased by several orders of magnitude in future work through a combination of high-sensitivity imaging detectors, high-numerical-aperture optics, increased optical fluence, and a forward-scattered geometry.

The downside of a miniaturized aerosol injector is that the small exit aperture, 100 µm diameter in our case, is prone to clogging. While these injectors can run

for many hours, clogging is typically observed whenever the liquid jet misbehaves and produces large droplets for a period of a few minutes. It is therefore essential to ensure the formation of small droplets and continuous flow of carrier gas. The severity of this issue could be greatly reduced by filtering out large droplets with, for example, an inline impactor. In the XFEL experiment reported here, there were a total of three clogged nozzles over a period of six hours.

SFX experiments using liquid jet injection typically obtain hit rates > 1 % for sample flow rate of about two fold higher than our measurement. As described above, we attribute much of the lower hit rates obtained in this study to misalignment and poor particle transport efficiency. In addition, aerosol particles injected from convergent nozzles typically travel with a speed > 250 m/s, compared to $10 - 20$ m/s for liquid jets. This difference alone accounts for a reduction of the observed hit rates by a factor of upto ~ 25. While these higher velocities are unfavorable for the present experiments at 120 Hz x-ray-pulse repetition rate, facilities that are currently under construction will offer MHz repetition rates and full utilization of such high repetition rates will require injections system which could deliver faster particles successively at least with a velocity of 100 m/s in order to provide undamaged crystals to every x-ray pulse.

5. Conclusions

We demonstrated x-ray diffraction from aerosolized sub-micrometer protein crystals with background levels drastically lower than in typical SFX experiments utilizing liquid jets. This will be important for coherent-diffractive-imaging experiments on weakly scattering targets such as isolated proteins, viruses, or cells, as well as for the measurement of diffuse or lattice-transform signals between crystalline Bragg reflections (Ayyer *et al.*, 2016; Kirian *et al.*, 2015*b*). We show that our injector is compatible with the existing hardware at LCLS, allowing quick changes from a liquid jet to an

aerosol injection system in a single experiment.

While the obtained hit fraction at LCLS was much lower than in typical liquid jet x-ray diffraction experiments, laboratory measurements suggest that this can be improved tremendously. Improved aerodynamic focusing will allow for further improvements (Roth *et al.*, 2016). Based on these laboratory measurements, we attribute the low hit fractions observed in this study to aerosol transport losses and misalignment between the x-ray focus and particle beam focus. In the future, performing SFX experiments from aerosolized crystals could provide a route for collecting extremely low background, high signal-to-noise diffraction patterns. Furthermore, due to the fast particle velocities and hence rapid replenishment of sample, our approach is compatible with upcoming high-repetition-rate FEL sources.

Acknowledgments

We thank the LCLS staff for accommodating laser-light-scattering imaging in the CXI instrument during our experiments. Portions of this research were carried out at the LCLS at the SLAC National Accelerator Laboratory. This LCLS beamtime was part of the Protein Crystal Screening (PCS) program. LCLS is an Office of Science User Facility operated for the US Department of Energy Office of Science by Stanford University. Use of the Linac Coherent Light Source (LCLS), SLAC National Accelerator Laboratory, is supported by the U. S. Department of Energy, Office of Science, Office of Basic Energy Sciences under Contract No. DE-AC02-76SF00515. Parts of the sample delivery system used at LCLS for this research was funded by the NIH grant P41GM103393, formerly P41RR001209.

In addition to DESY, this work has been supported by the excellence cluster "The Hamburg Center for Ultrafast Imaging–Structure, Dynamics and Control of Matter at the Atomic Scale" of the Deutsche Forschungsgemeinschaft (CUI, DFG-EXC1074), the European Research Council through the Consolidator Grant COMOTION (ERC-

614507-Küpper), the Helmholtz Association "Initiative and Networking Fund", and the Australian Research Council's Discovery Projects funding scheme (DP110100975). R.A.K. acknowledges support from an NSF STC Award (1231306).

References

Aquila, A., Barty, A., Bostedt, C., Boutet, S., Carini, G., DePonte, D., Drell, P., Doniach, S., Downing, K. H., Earnest, T., Elmlund, H., Elser, V., Gühr, M., Hajdu, J., Hastings, J., Hau-Riege, S. P., Huang, Z., Lattman, E. E., Maia, F. R. N. C., Marchesini, S., Ourmazd, A., Pellegrini, C., Santra, R., Schlichting, I., Schroer, C., Spence, J. C. H., Vartanyants, I. A., Wakatsuki, S., Weis, W. I. & Williams, G. J. (2015). *Struct. Dyn.* **2**(4), 041701.

Awel, S., Kirian, R. A., Eckerskorn, N., Wiedorn, M., Horke, D. A., Rode, A. V., Küpper, J. & Chapman, H. N. (2016). *Opt. Exp.* **24**(6), 6507–6521.

Ayyer, K., Yefanov, O. M., Oberthür, D., Roy-Chowdhury, S., Galli, L., Mariani, V., Basu, S., Coe, J., Conrad, C. E., Fromme, R., Schaffer, A., Dörner, K., James, D., Kupitz, C., Metz, M., Nelson, G., Xavier, P. L., Beyerlein, K. R., Schmidt, M., Sarrou, I., Spence, J. C. H., Weierstall, U., White, T. A., Yang, J.-H., Zhao, Y., Liang, M., Aquila, A., Hunter, M. S., Robinson, J. S., Koglin, J. E., Boutet, S., Fromme, P., Barty, A. & Chapman, H. N. (2016). *Nature*, **530**(7589), 202–206.
URL: *http://www.nature.com/doifinder/10.1038/nature16949*

Barty, A., Küpper, J. & Chapman, H. N. (2013). *Annu. Rev. Phys. Chem.* **64**(1), 415–435.
URL: *http://dx.doi.org/10.1146/annurev-physchem-032511-143708*

Beyerlein, K. R., Adriano, L., Heymann, M., Kirian, R., Knoska, J., Wilde, F., Chapman, H. N. & Bajt, S. (2015). *Rev. Sci. Instrum.* **86**(12), 125104–12.

Bogan, M. J., Benner, W. H., Boutet, S., Rohner, U., Frank, M., Barty, A., Seibert, M. M., Maia, F., Marchesini, S., Bajt, S., Woods, B., Riot, V., Hau-Riege, S. P., Svenda, M., Marklund, E., Spiller, E., Hajdu, J. & Chapman, H. N. (2008). *Nano Letters*, **8**(1), 310–316.
URL: *http://pubs.acs.org/cgi-bin/abstract.cgi/nalefd/2008/8/i01/abs/nl072728k.html*

Bogan, M. J., Boutet, S., Chapman, H. N., Marchesini, S., Barty, A., Benner, W. H., Rohner, U., Frank, M., Hau-Riege, S. P., Bajt, S., Woods, B., Seibert, M. M., Iwan, B., Timneanu, N., Hajdu, J. & Schulz, J. (2010*a*). *Aerosol Sci. Techn.* **44**(3), i–vi.

Bogan, M. J., Starodub, D., Hampton, C. Y. & Sierra, R. G. (2010*b*). *J. Phys. B*, **43**(19), 194013.
URL: *http://iopscience.iop.org/0953-4075/43/19/194013*

Boutet, S., (2016). private communication.

Boutet, S., Lomb, L., Williams, G. J., Barends, T. R. M., Aquila, A., Doak, R. B., Weierstall, U., DePonte, D. P., Steinbrener, J., Shoeman, R. L., Messerschmidt, M., Barty, A., White, T. A., Kassemeyer, S., Kirian, R. A., Seibert, M. M., Montanez, P. A., Kenney, C., Herbst, R., Hart, P., Pines, J., Haller, G., Gruner, S. M., Philipp, H. T., Tate, M. W., Hromalik, M., Koerner, L. J., van Bakel, N., Morse, J., Ghonsalves, W., Arnlund, D., Bogan, M. J., Caleman, C., Fromme, R., Hampton, C. Y., Hunter, M. S., Johansson, L. C., Katona, G., Kupitz, C., Liang, M., Martin, A. V., Nass, K., Redecke, L., Stellato, F., Timneanu, N., Wang, D., Zatsepin, N. A., Schafer, D., Defever, J., Neutze, R., Fromme, P., Spence, J. C. H., Chapman, H. N. & Schlichting, I. (2012). *Science*, **337**(6092), 362–364.
URL: *http://www.sciencemag.org/content/337/6092/362.abstract*

Chapman, H. N., Fromme, P., Barty, A., White, T. A., Kirian, R. A., Aquila, A., Hunter, M. S., Schulz, J., Deponte, D. P., Weierstall, U., Doak, R. B., Maia, F. R. N. C., Martin, A. V., Schlichting, I., Lomb, L., Coppola, N., Shoeman, R. L., Epp, S. W., Hartmann, R., Rolles, D., Rudenko, A., Foucar, L., Kimmel, N., Weidenspointner, G., Holl, P., Liang, M., Barthelmess, M., Caleman, C., Boutet, S., Bogan, M. J., Krzywinski, J., Bostedt, C., Bajt, S., Gumprecht, L., Rudek, B., Erk, B., Schmidt, C., Hömke, A., Reich, C., Pietschner, D., Strüder, L., Hauser, G., Gorke, H., Ullrich, J., Herrmann, S., Schaller, G., Schopper, F., Soltau, H., Kühnel, K.-U., Messerschmidt, M., Bozek, J. D., Hau-Riege, S. P., Frank, M., Hampton, C. Y., Sierra, R. G., Starodub, D., Williams, G. J., Hajdu, J., Timneanu, N., Seibert, M. M., Andreasson, J., Rocker, A., Jönsson, O., Svenda, M., Stern, S., Nass, K., Andritschke, R., Schröter, C.-D., Krasniqi, F., Bott, M., Schmidt, K. E.,

Wang, X., Grotjohann, I., Holton, J. M., Barends, T. R. M., Neutze, R., Marchesini, S., Fromme, R., Schorb, S., Rupp, D., Adolph, M., Gorkhover, T., Andersson, I., Hirsemann, H., Potdevin, G., Graafsma, H., Nilsson, B. & Spence, J. C. H. (2011). *Nature*, **470**(7332), 73.
URL: *http://www.nature.com/nature/journal/v470/n7332/full/nature09750.html*

DePonte, D. P., Weierstall, U., Schmidt, K., Warner, J., Starodub, D., Spence, J. C. H. & Doak, R. B. (2008). *J. Phys. D*, **41**(19), 195505.
URL: *http://iopscience.iop.org/0022-3727/41/19/195505*

Frank, M., Carlson, D. B., Hunter, M. S., Williams, G. J., Messerschmidt, M., Zatsepin, N. A., Barty, A., Benner, W. H., Chu, K., Graf, A. T., Hau-Riege, S. P., Kirian, R. A., Padeste, C., Pardini, T., Pedrini, B., Segelke, B., Seibert, M. M., Spence, J. C. H., Tsai, C. J., Lane, S. M., Li, X. D., Schertler, G., Boutet, S., Coleman, M. & Evans, J. E. (2014). *IUCrJ*, **1**, 95–100.

Gati, C., Oberthuer, D., Yefanov, O., Bunker, R. D., Stellato, F., Chiu, E., Yeh, S.-M., Aquila, A., Basu, S., Bean, R., Beyerlein, K. R., Botha, S., Boutet, S., DePonte, D., Doak, R. B., Fromme, R., Galli, L., Grotjohann, I., James, D. R., Kupitz, C., Lomb, L., Messerschmidt, M., Nass, K., Rendek, K., Shoeman, R. L., Wang, D., Weierstall, U., White, T. A., Williams, G. J., Zatsepin, N. A., Fromme, P., Spence, J., Goldie, K. N., Jehle, J. A., Barty, A., Metcalf, P. & Chapman, H. N. (2017). *Proc. Natl. Acad. Sci. U.S.A.* In press.

Jehle, J. A., Lange, M., Wang, H., Hu, Z., Wang, Y. & Hauschild, R. (2006). *Virol. J*, **346**(1), 180–193.

Kirian, R. A., Awel, S., Eckerskorn, N., Fleckenstein, H., Wiedorn, M., Adriano, L., Bajt, S., Barthelmess, M., Bean, R., Beyerlein, K. R., Chavas, L. M. G., Domaracky, M., Heymann, M., Horke, D. A., Knoska, J., Metz, M., Morgan, A., Oberthuer, D., Roth, N., Sato, T., Xavier, P. L., Yefanov, O., Rode, A. V., Küpper, J. & Chapman, H. N. (2015*a*). *Struct. Dyn.* **2**(4), 041717.

Kirian, R. A., Bean, R. J., Beyerlein, K. R., Barthelmess, M., Yoon, C. H., Wang, F., Capotondi, F., Pedersoli, E., Barty, A. & Chapman, H. N. (2015*b*). *Phys. Rev. X*, **5**(1), 011015–12.

Küpper, J., Stern, S., Holmegaard, L., Filsinger, F., Rouzée, A., Rudenko, A., Johnsson, P., Martin, A. V., Adolph, M., Aquila, A., Bajt, S., Barty, A., Bostedt, C., Bozek, J., Coleman, C., Coffee, R., Coppola, N., Delmas, T., Epp, S., Erk, B., Foucar, L., Gorkhover, T., Gumprecht, L., Hartmann, A., Hartmann, R., Hauser, G., Holl, P., Hömke, A., Kimmel, N., Krasniqi, F., Kühnel, K.-U., Maurer, J., Messerschmidt, M., Moshammer, R., Reich, C., Rudek, B., Santra, R., Schlichting, I., Schmidt, C., Schorb, S., Schulz, J., Soltau, H., Spence, J. C. H., Starodub, D., Strüder, L., Thøgersen, J., Vrakking, M. J. J., Weidenspointner, G., White, T. A., Wunderer, C., Meijer, G., Ullrich, J., Stapelfeldt, H., Rolles, D. & Chapman, H. N. (2014). *Phys. Rev. Lett.* **112**, 083002.

Liang, M., Williams, G. J., Messerschmidt, M., Seibert, M. M., Montanez, P. A., Hayes, M., Milathianaki, D., Aquila, A., Hunter, M. S., Koglin, J. E. *et al.* (2015). *J. Synchrotron Rad.* **22**(3), 514–519.

Muniyappan, S., Kim, S. & Ihee, H. (2015). *Bio Design*, **3**(2), 98–110.

Neutze, R., Wouts, R., van der Spoel, D., Weckert, E. & Hajdu, J. (2000). *Nature*, **406**(6797), 752–757.
URL: *http://dx.doi.org/10.1038/35021099*

Oberthür, D., Knoska, J., Wiedorn, M., Beyerlein, K., Bushnell, D., Kovaleva, E., Heymann, M., Gumprecht, L., Kirian, R., Barty, A., Mariani, V., Tolstikova, A., White, T., Adriano, L., Awel, S., Barthelmes, M., Drner, K., Paulraj, L. X., Yefanov, O., James, D., Chen, J., Nelson, G., Wang, D., Echelmeier, A., Abdallah, B., Ros, A., Calvey, G., Chen, Y., Frielingsdorf, S., Lenz, O., Schmidt, A., Szczepek, M., Snell, E., Robinson, P., arler, B., Belsak, G., Macek, M., Wilde, F., Aquila, A., Boutet, S., Liang, M., Hunter, M., Scheerer, P., Libscomb, J. D., Weierstall, U., Kornberg, R., Spence, J., Pollack, L., Chapman, H. N. & Bajt, S. (2016). *Sci. Rep.* Submitted.

Patterson, B. D. (2014). *Crystallogr. Rev.* **20**(4), 242–294.

Roth, N., Horke, D. A., Awel, S. & Küpper, J. (2016). In preparation.

Schlichting, I. (2015). *IUCrJ*, **2**(2), 246–255.

Schlichting, I. & Miao, J. (2012). *Curr. Opin. Struct. Biol.* **22**(5), 613–626.

Spence, J. C. H., Kirian, R. A., Wang, X., Weierstall, U., Schmidt, K. E., White, T., Barty, A., Chapman, H. N., Marchesini, S. & Holton, J. (2011). *Opt. Exp.* **19**(4), 2866.

Spence, J. C. H., Weierstall, U. & Chapman, H. N. (2012). *Rep. Prog. Phys.* **75**(10), 102601. **URL:** *http://dx.doi.org/10.1088/0034-4885/75/10/102601*

Weierstall, U. (2014). *Phil. Trans. R. Soc. B*, **369**(1647), 20130337–20130337.

Weierstall, U., James, D., Wang, C., White, T. A., Wang, D., Liu, W., Spence, J. C. H., Bruce Doak, R., Nelson, G., Fromme, P., Fromme, R., Grotjohann, I., Kupitz, C., Zatsepin, N. A., Liu, H., Basu, S., Wacker, D., Won Han, G., Katritch, V., Boutet, S., Messerschmidt, M., Williams, G. J., Koglin, J. E., Marvin Seibert, M., Klinker, M., Gati, C., Shoeman, R. L., Barty, A., Chapman, H. N., Kirian, R. A., Beyerlein, K. R., Stevens, R. C., Li, D., Shah, S. T. A., Howe, N., Caffrey, M. & Cherezov, V. (2014). *Nat. Commun.* **5**.

Weierstall, U., Spence, J. & Doak, R. (2012). *Rev. Sci. Instrum.* **83**(3), 035108.

White, T. A., Kirian, R. A., Martin, A. V., Aquila, A., Nass, K., Barty, A. & Chapman, H. N. (2012). *J. Appl. Cryst.* **45**(2), 335–341.

Yang, J., Guehr, M., Shen, X., Li, R., Vecchione, T., Coffee, R., Corbett, J., Fry, A., Hartmann, N., Hast, C., Hegazy, K., Jobe, K., Makasyuk, I., Robinson, J., Robinson, M. S., Vetter, S., Weathersby, S., Yoneda, C., Wang, X. & Centurion, M. (2016). *Phys. Rev. Lett.* **117**, 153002.

Synopsis

A new approach is demonstrated that achieves very low background in the measurement of diffraction from macromolecular nanocrystals by using an aerosol focusing injector with an x-ray free-electron laser.